

Composition-induced microstructures in rhombohedral carbonates

D. J. BARBER AND M. RIAZ KHAN

Physics Department, University of Essex, Wivenhoe Park, Colchester, Essex CO4 3SQ

Abstract

Recent TEM observations of two-phase microstructures and associated crystal defects in selected, rare dolomites have been extended to calcite-structured ($R\bar{3}c$) carbonates and to other natural and synthetic carbonates that crystallize with the dolomite ($R\bar{3}$) structure. The samples included siderites (FeCO_3), smithsonites (ZnCO_3), ankerites ($\text{Ca}[\text{Mg,Fe}](\text{CO}_3)_2$), and kutnahorites ($\text{Ca}[\text{Mn,Fe}](\text{CO}_3)_2$).

TEM methods show that the forms of second phases which result from the presence of common, divalent, metallic impurities are morphologically similar in $R\bar{3}c$ and $R\bar{3}$ carbonates and occur more widely than hitherto realized. The most common form consists of thin ribbons of second phase which are coherent with and have the same crystallographic orientation as the host carbonate. Another form of microstructure, manifest as modulations in diffraction contrast, appears to be associated with incipient breakdown of single-phase carbonate. The results of extensive TEM/EDS microanalyses show that in siderite and ankerite the formation of ribbons is promoted by Ca impurity or Ca excess (with respect to $R\bar{3}c$ stoichiometry). In smithsonite, Cu and Ca impurities can play similar roles in relation to modulated microstructures. In kutnahorites, the perfection of grains and the absence of second-phase effects is strongly dependent on the ratio of Fe to Mn but is also affected by Ca in excess of the stoichiometric requirement. Electron diffraction results from several of the minerals show c -type spots, which can be interpreted as indicating ordering within basal layers of cations.

The results show that, by correlating analytical TEM data with the study of second phases and incipient two-phase microstructures, it should be possible to determine the limits of solid solubility in carbonate systems.

KEYWORDS: microstructures, rhombohedral carbonates, siderite, smithsonite, ankerite, kutnahorite.

Introduction

THE application of TEM methods to the study of possible relationships between chemical composition and microstructure in two relatively rare types of dolomite, $\text{CaMg}(\text{CO}_3)_2$ has already indicated that a Ca/Mg ratio greater than unity can result in the local formation of a finely distributed calcitic second phase. For example, in calcian 'saddle dolomite' (characteristic low-temperature growths of distorted crystals—Radke and Mathis, 1980) the second phase appears (Barber *et al.*, 1985) as ubiquitous, thin, twisting and branching ribbons, which are often or generally crystallographically coherent with the host dolomite. The composition of dolomite within the Alnø and Fen carbonatites is more variable, but grains of dolomite and ankerite with a Ca/(Mg+Fe) ratio greater than unity frequently contain ribbons that are morphologically similar (Barber and Wenk, 1984) to those in the

saddle dolomites. The nature of the ribbons in both cases has been inferred from electron diffraction and X-ray analytical data and has been supported by analysis and simulation (King *et al.*, 1984) of the fringe diffraction contrast shown by the ribbons.

Dolomite and calcite have very similar crystal structures (Reeder, 1983a), the former having a lower symmetry ($R\bar{3}$) than the latter ($R\bar{3}c$), on account of the ordered arrangement of alternating layers of dissimilar A, B cations parallel to the basal planes. The a and c lattice parameters of dolomite and calcite differ by about 3.6 and 6.2 percent respectively, so that it is easy to understand both the good coherency between the two lattices at the ribbon-host interfaces and the lack of crystallographic control over the interfacial 'plane', which loosely favours $\{10\bar{1}4\}$.

The work described here extends the study of fine-scale, apparently two-phase, effects to other rhombohedral carbonate minerals, including some

with the calcite structure. It also contains a few preliminary results obtained from carbonates synthesized by solid-state sintering, which will be used to study composition-microstructure relationships systematically.

Dolomites of medium-to-high metamorphic grade usually have very nearly perfect cation ordering. Only non-stoichiometric, sedimentary dolomites normally give X-ray and electron-diffraction patterns indicative of significant degrees of disorder (Reeder and Wenk, 1979*a, b*). (However, it can be argued that electron diffraction does not give information about substitutional order.) The manner in which the dolomite structure may accommodate small departures from ideal A, B cation stoichiometry has been suggested in an interpretation of lattice images obtained by high-resolution transmission electron microscopy (HREM) (Van Tendeloo *et al.*, 1985) of sequential, basal faults (Wenk and Zenger, 1983) that occur in unique crystals from the Lost Burro Formation, California. This suggests that the so-called 'c-type' reflections (corresponding to a lattice with $a = 2a_{\text{DOL}}$) which were first reported (Reeder and Wenk, 1978*a, b*; Reeder, 1981) as occurring in the electron diffraction patterns from Ca-rich sedimentary dolomites, are a result of the ordering of cations within a basal layer. The various types of electron diffraction spots are denoted in the following ways:

Spots corresponding to allowed reflections for the $R\bar{3}c$ symmetry are called 'a-type' spots, while those corresponding to the extra ordering reflections arising from the $R\bar{3}$ symmetry are called 'b-type' spots. The 'c-type' spots in the diffraction patterns are then found at positions halfway between the 'a-type' spots; their presence indicates the loss of rhombohedral symmetry. It has been proposed by Van Tendeloo *et al.* (1985) that 'd-type' reflections (at positions corresponding to $-h+k+l \neq 3n$) in diffraction patterns from the Lost Burro dolomite arise from a periodic stacking of basal layers which gives not a rhombohedral structure, but one that is hexagonal.

The foregoing ideas have not been widely tested, but they help to focus attention on the various possibilities that may exist close to the phase boundaries in carbonate systems. Detailed phase diagrams do not exist for most mixed carbonate systems (the best data have been summarized quite recently—Goldsmith, 1983) but information about the extent of solid solubility, factors influencing phase stability, partitioning, etc., in some of the lesser-known systems is now appearing (e.g. Rosenberg and Foit, 1979; Effenberger *et al.*, 1981; Lloyd *et al.*, 1985). In this field analytical TEM/STEM methods have much to contribute and our results are a first attempt at assessing what problems

may be encountered and in establishing whether there are common aspects to the microstructural manifestations of single-phase breakdown in the rhombohedral carbonates.

Experimental methods, origins and types of samples

Since only small quantities of the minerals were available, our methods of study were restricted to optical petrography of thin sections and TEM techniques. Regions of interest were noted in the thin sections, which were then demounted so that pieces of them could be fixed to '7-HEX' electron microscope grids with epoxy cement. Ion-thinning was then carried out at 5.5 kV, using low current densities of argon ions to minimize heating and to avoid excessive amorphization of the specimen surfaces.

The minerals with the dolomite structure were ankerites and kutnahorites, those with the calcite structure were calcite, siderite and smithsonite. The origins of the samples are given in the relevant sections and their sources appear in the acknowledgements. The synthetic rhombohedral carbonates in the MnCO_3 - CaCO_3 and MgCO_3 - CdCO_3 systems are being made at Essex University starting from reagent-grade anhydrous carbonate powders. The latter are mixed in appropriate molar ratios, adding 1% Li_2CO_3 to assist sintering. After drying at about 60 °C, the powders are remixed and then encapsulated in rubber dies and cold-pressed isostatically at 0.15 MPa. The resulting powder compacts are sealed into gas-tight, thin-walled, platinum tubes. Solid-state sintering is carried out using an internally heated, high-pressure vessel held at pressures of the order of 0.3 MPa for times of ~ 10–30 hr.

The electron microscope used was a JEOL 200-CX, which was operated at 200 kV for imaging and diffraction operations, and at 120 kV for X-ray microanalysis. The latter was carried out by means of a high take-off angle detector linked to a quantitative spectrum-processing system. Most of the analyses were carried out in the TEM mode on untilted specimens, utilizing the reduced electron-probe diameters that are possible with free control of the electron lenses.

With the exception of that for Mn, the k -factors (Cliff and Lorimer, 1975; Wood *et al.*, 1984) used in processing the X-ray spectra were experimentally determined and normalized to Fe, using well-quantified thin-section standards. The factor for Mn was interpolated from the factors of adjacent elements, using a theoretical relationship (Cliff and Lorimer, 1975). Individual compositional analyses are estimated from checks on standards to have an absolute accuracy of between 0.5 and 1.0 per cent,

relative to the amount of element present. Comparative accuracy between TEM/EDS analyses is better than 0.5 per cent, as judged from the counting statistics.

Results

Ankerite

Three of the ankerites available to us contain significant amounts of a second-phase carbonate. The samples originated from Muzo, Boyaca, Colombia (BM 1948, 86), Neudorf, Harz, Germany (BM 83816), Londonderry, Colchester County, Nova Scotia (BM 1917, 128) and from the Alnø and Fen carbonatites (Von Eckermann, 1948; see also Barber and Wenk, 1984). Of these, the sample from Neudorf exhibits some of the best examples of ribbon- or lath-like second phase that we have yet found in an R3 carbonate. Both the ribbon density and the thicknesses of some of the ribbons lead to greater ease in studying them than is usually encountered. TEM/EDS gives the range of compositions for ribbon-free volumes as 9–10 mole % MgO; 49–50.5 mole % CaO; 7–8 mole % MnO; 33–35 mole % FeO.

Bright-field (BF) and dark-field (DF) images of well-spaced ribbon defects in very thin regions of

Neudorf ankerite enable the nature of the diffraction contrast to be studied in detail. It is found that the fringes shown by the ribbons are essentially complementary—extreme fringes are dark and symmetric in BF, light and symmetric in DF. The properties of the fringes are consistent with the ribbons being thin layers of a phase which is lattice-coherent with the host crystal (King *et al.*, 1984) and the ribbons are therefore essentially similar to the ribbons of carbonate second phase already observed in both saddle dolomites (Barber *et al.*, 1985) and carbonatitic dolomite (Barber and Wenk, 1984). In very thin (~ 100 nm) parts of the ankerite the three-dimensional relationships between the ribbons, and their typical interconnecting or branching character is not apparent. It is exemplified, for the Neudorf ankerite, by Fig. 1a and b, which are corresponding BF and DF images. These illustrate that the ribbons sometimes form a semi-continuous microstructure of equiaxed polygonal cell-walls (somewhat like grain boundaries in a well-annealed material), with no significant misorientation between cells over the visible fields. Even where such a regular, cellular arrangement does not occur, the TEM images suggest that the thin sheets of second-phase material, manifest as laths in the ion-thinned sections, often link to form

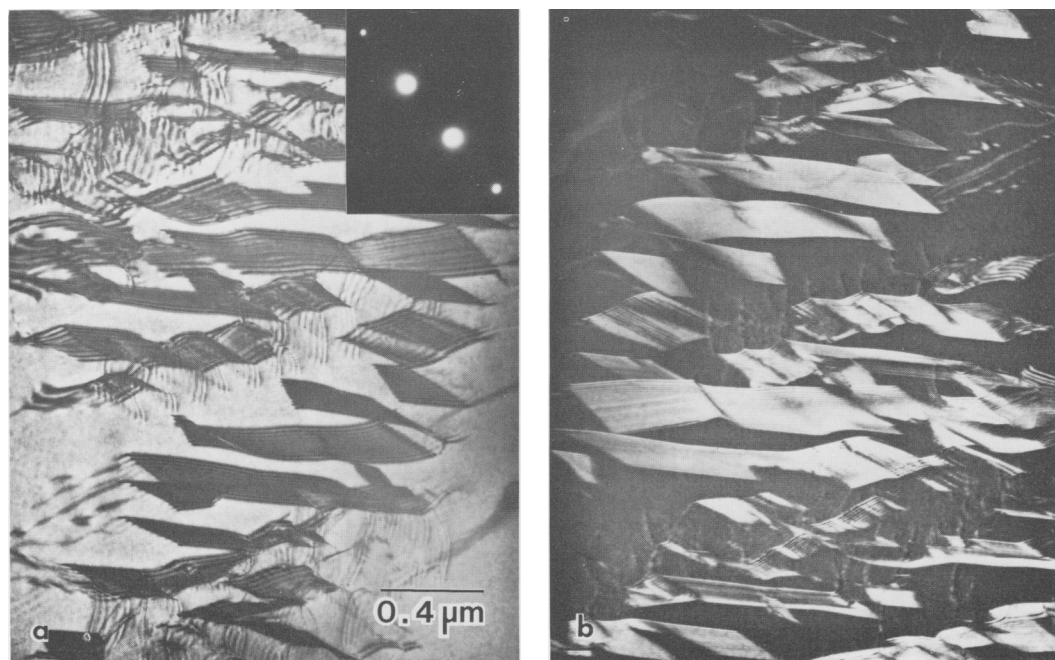


FIG. 1 (a and b). BF and DF images of interlinked ribbons of calcitic second-phase in Neudorf ankerite, using a 10 $\bar{1}$ 4 reflection.

a semicontinuous microstructure within the ankerite grains.

Direct evidence concerning the identity of the second phase in ankerite cannot be obtained for every region exhibiting the fringed ribbons. Analysis of regions showing a high ribbon density, using comparable instrumental conditions, invariably shows a higher Ca content and often a lower Mn content, the results being dependent on the volume fraction of second-phase laths in the area

under the electron beam (typically $1-5 \mu\text{m}^2$). This 'broad-beam' TEM/EDS method of establishing trends when comparing analyses of 'clear' (i.e. ribbon- or striation-free) regions and second-phase regions will be subsequently termed the 'average composition method'. It was generally less conclusive with the ankerite samples than with the other carbonates because of the low volume-fraction of second phase in the ankerites (i.e. widely spaced ribbons).

It is possible, in principle, to improve upon the averaging effect of carrying out TEM microanalysis over a ribbon-dense region by using a STEM probe to analyse a ribbon that has been tilted into an 'edge-on' orientation. This method is laborious because it requires long counting times, good probe stability and especially thick ribbons to be really successful. The procedure is illustrated by Fig. 2. The chosen ribbon (here a short, thick one) is shown untilted (Fig. 2a), then tilted into the orientation for STEM analysis (Fig. 2b—note that only the part at the arrow, the point of analysis, is truly 'edge on'), and then tilted back after analysis to show that the contamination spots on upper and lower surfaces straddle the second-phase ribbon (Fig. 2c). The results of several typical STEM analyses are given in Table 1. They indicate no reproducible change in Fe content but a reproducible change in Ca content between the probed position on the ribbon and the adjacent material, with the trend always in the same sense. With respect to the host ankerite, the ribbon position is Ca-rich and tends to be Mn-poor. However, such analyses do not give the composition of the ribbons, because the probe diameter ($\sim 20 \text{ nm}$) is of the same order as the thickness of the thickest ribbons and considerably

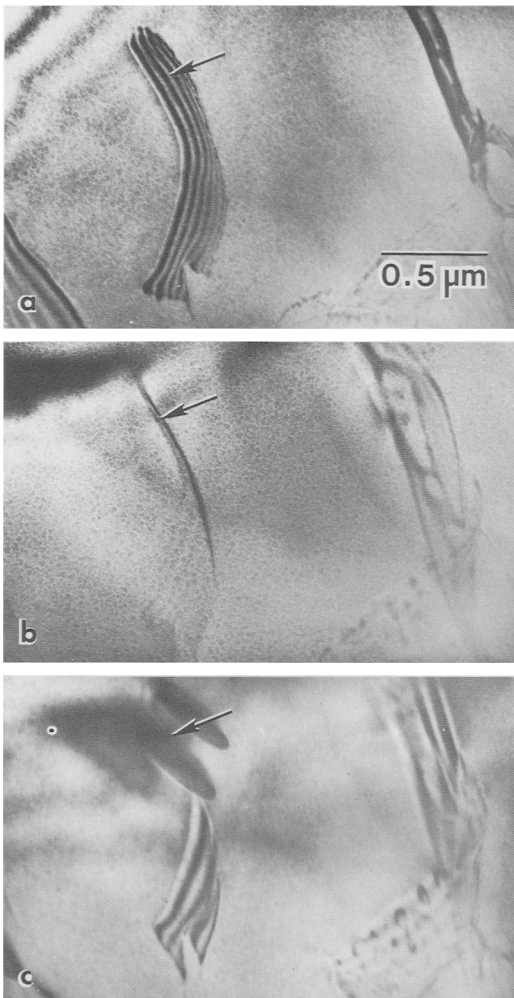


FIG. 2 (a-c). Illustrating the STEM analysis of a second-phase ribbon in Neudorf ankerite. In (b) one end of the ribbon has been tilted into an 'edge on' orientation and in (c) it is tilted again to show that the two spots (on upper and lower surfaces of the specimen) produced by contamination under the STEM probe are positioned on either side of the part of the ribbon analysed.

TABLE 1

Showing the results of some typical STEM/EDS microanalyses recorded with the electron probe situated on (A) a ribbon and, (B) within a "clear" region in the Neudorf ankerite. The four main divalent metal carbonates present are assumed to total 100 percent.

	A (wt. % oxide)				B (wt. % oxide)			
	MgO	CaO	MnO	FeO	MgO	CaO	MnO	FeO
9.75	49.51	6.58	34.16	10.98	48.45	7.25	33.32	
9.96	50.18	6.43	33.43	10.28	47.65	7.45	34.62	
9.97	49.48	6.65	33.90	10.70	48.75	6.77	33.78	
10.33	50.14	6.65	32.88	11.06	48.40	6.55	33.99	
10.08	51.08	6.39	32.45	9.59	49.44	7.01	33.96	
9.65	49.35	7.28	33.72	10.01	48.70	7.17	34.12	
9.11	49.05	7.22	34.62	11.59	47.49	7.03	33.89	
8.98	50.12	6.87	34.03	9.48	49.39	7.08	34.05	

greater than that of the majority, to judge from lattice images. Beam-spreading effects, coupled with uncertainties in the exact positions, thicknesses and orientations of the ribbons inevitably means that the volume for X-ray production always includes much host material. Great weight must therefore be placed on less direct evidence concerning the second phase, as follows.

Examination of high-order diffraction spots frequently reveals a small splitting of the spots, indicative of a second lattice topotactic with the ankerite lattice, and the reflections due to ordering are somewhat diminished in intensity. DF imaging with the 'split reflections' produces Moiré patterns at the ribbon/host interfaces. The best fit to the subsidiary reciprocal lattice is a mineral with symmetry $R\bar{3}$. If the second-phase spot of one of the high-order reflections is used for DF imaging (by means of a very small objective aperture), only the ribbons appear bright. All these findings point to the second phase being not only Ca-rich, but calcite itself.

Kutnahorite

The samples originated from Kutna Hora, Bohemia (BM 1969, 283), Broken Hill, New South

Wales (BM 1974, 288), Chvaltice, Bohemia (see Zak and Povondra, 1981), and Piz Cam, Bergell Alps, Switzerland (see Wenk and Maurizio, 1978). According to Goldsmith (1983) kutnahorite ideally has the composition $\text{CaMn}(\text{CO}_3)_2$, but the four samples that we have studied contained significant amounts of Mg and Fe.

All four samples show various two-phase and incipient two-phase effects, but two composition-related microstructures are easily recognized and are apparently characteristic. These are seen in the TEM as (i) modulations and/or striations in diffraction contrast, (ii) lattice-coherent ribbons or laths of a second phase. The former often occur together with many dislocations, but the nature and origins of the latter are hard to elucidate on account of local elastic strains. Sub-grain boundaries and other arrays of dislocations also often occur in apparently single-phase regions which are frequently adjacent to type (i) regions.

One sample, from the type locality, Kutna Hora, Bohemia, appears from the restricted sampling possible by TEM methods to have no single-phase material, and it has both intense modulation and high densities of ribbon defects, sometimes intermingled. Significant volume fractions of the

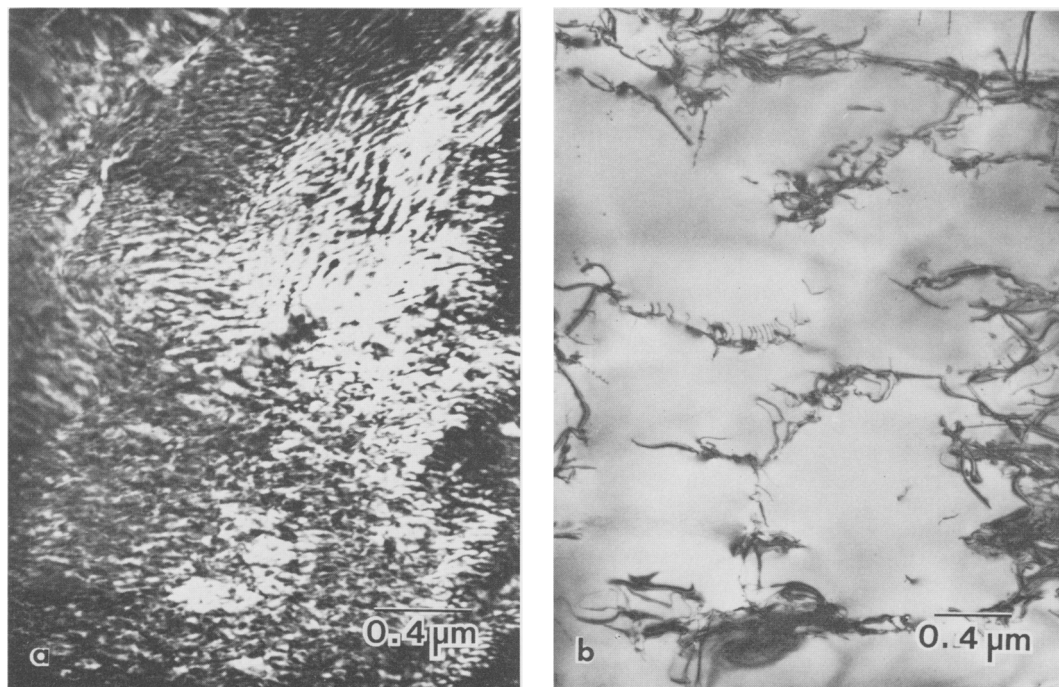


FIG. 3 (a and b). DF and BF images, respectively, of (a) striated region and (b) unstriated region in Chvaltice kutnahorite.

other three samples, on which we have concentrated, are free from composition-induced defect microstructures and contain what we assume to be 'normal' single-phase kutnahorite, with relatively low densities of dislocations ($\sim 10^3 \text{ cm}^{-2}$). However, the three minerals are somewhat heterogeneous, so that both composition and microstructure change on a scale of 10–100 μm . The variations in composition are most readily manifest as changes in the Mn/Fe ratio, often matched with smaller changes in Mg and Ca contents. The sample from Chvaletice, Eastern Bohemia has already been reported by Zak and Povondra (1981) as showing quasi-regular compositional variations on a scale of the order of 10 μm . These authors noted a prevailing Fe+Ca versus Mn+Mg antagonism in all the kutnahorites from Chvaletice used in their study and they also deduced by means of X-ray diffraction that one specimen contained two related carbonate phases.

We now consider how the two main microstructures that we find relate to the local composition of the kutnahorites.

Qualitative correlation between composition and microstructures. Fig. 3a shows a modulated or striated region in the Bergell kutnahorite while, for comparison, Fig. 3b shows an adjacent region which was free of striations and merely contains an irregular, cellular structure of dislocations. The selected area diffraction pattern for Fig. 3a corresponds to $R\bar{3}$ symmetry and shows no *c*-type spots. X-ray microanalysis of this and similarly striated regions established reproducibly that the striated regions in all the kutnahorite samples have different compositions from those of the closely adjacent regions that are free of striations or contrast modulations (hereafter called 'clear' regions, for brevity). In particular, the ribbon regions have higher Fe/Ca and lower Mn/Ca ratios than the adjacent clear regions. Qualitatively speaking, similar effects are found in Chvaletice kutnahorite. Fig. 4 shows EDS spectra recorded at positions within striated and clear regions of that material which were separated by about 10 μm . It is apparent that there is much less Fe and more Mn in the clear region, while the Mg contents are similar. (It should be noted that, because of the variation of detector efficiency with X-ray energy and overlap of the Fe- $K\alpha$ and Mn- $K\beta$ peaks, the peak areas are not directly representative of concentration).

Ribbons of second phase are not equally common in three of the samples available to us, but they are widespread and closely associated with modulated microstructures in the sample of kutnahorite from Kutna Hora. This mineral has a very low Fe content ($\sim 1 \text{ wt. \% FeO}$), a fairly high Mg content and the Ca content exceeds the formula total of Fe,

Mg and Mn. The regions with well-developed ribbons have higher Mg and Ca contents than the regions which only show contrast modulations. The diffraction patterns from the modulated regions have sharp *b*-type spots. Currently we find this sample more difficult to interpret than the other kutnahorites, so we shall concentrate on results from them.

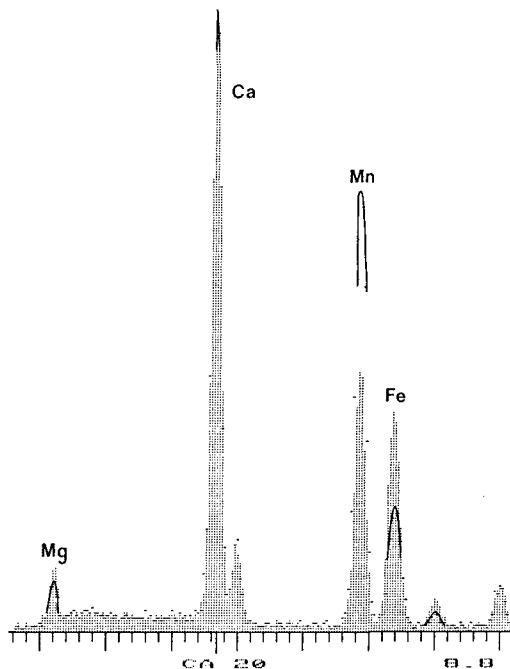


FIG. 4. Superposed TEM/EDS spectra corresponding to striated and unstriated regions in Chvaletice kutnahorite like those shown in Fig. 3 (*a* and *b*). Note the relative heights of the Mn and Fe peaks; the shaded spectrum is from the striated region and the outline spectrum (peaks picked out for clarity) is from the unstriated region. Total Ca counts are the same for the two spectra.

Comparisons of compositional analyses of single-phase and two-phase regions. In view of the apparent dependence of microstructure on composition reported above, we have obtained analytical data by probing statistically significant numbers of single-phase regions and apparently two-phase regions. (We apply the latter term to regions exhibiting either ribbons or contrast modulations.) The data were then examined for compositional correlations and the results were then plotted in terms of various elements that showed correlations. Some of these results now follow.

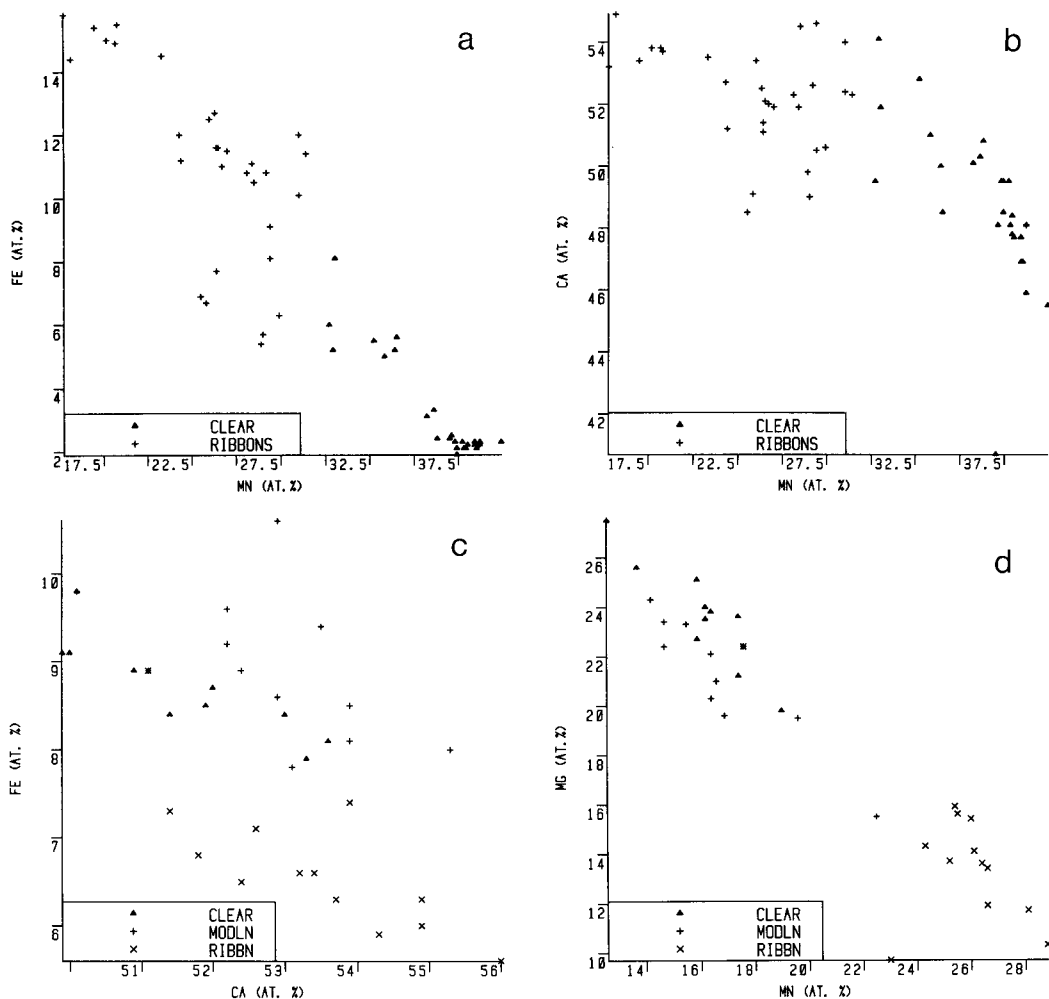


FIG. 5 (*a-d*). Graphs showing the results of TEM/EDS microanalyses giving (*a*) Fe versus Mn, and (*b*) Ca versus Mn, for single-phase ('clear') and two-phase ('ribbon') regions in the Chvaletice kutnahorite. (*c*) Fe versus Ca, and (*d*) Mg versus Mn, for single-phase ('clear'), incipient two-phase ('modulated') and two-phase ('ribbon') regions in the Bergell kutnahorite.

Fig. 5*a* and *b* show plots of Fe versus Mn, and Ca versus Mn respectively for analyses of clear and two-phase regions in the Chvaletice sample. In both graphs the data fall into two distinct groups. In terms of the Fe/Mn ratio particularly, there is an obvious trend in compositions and it appears that the second-phase carbonate is not only calcitic, but also contains significant Fe. From such figures it appears that it should be possible to estimate the concentrations of the main divalent cations which constitute the limits of solid solubility.

Similar analyses of clear and two-phase regions in the sample from the Bergell Alps at first pro-

duced three clusters of data points but one of these, corresponding to two-phase material, plotted directly adjacent to the cluster for the clear regions. The reason for this result became apparent when more analyses were undertaken and plotted, but taking care to distinguish between (1) data corresponding to the ribbon regions and (2) data for modulated regions or regions where the nature of the microstructure was uncertain (usually because of very high local densities of dislocations). Figs. 5*c* and *d* show plots of these data points, together with those for single phase regions, expressed in terms of Fe versus Ca, and the Mg versus Mn. It appears

that, in terms of average composition, the ribbon regions are low in Mg and high in Ca and Fe compared with both the single phase material and the modulated regions. This again points to the ribbons being calcitic. However, the modulated regions and those with unresolvable microstructures also have higher Mg/Mn ratios than the ribbon regions and indeed have Mg/Mn ratios that border those of the clear, presumably single-phase, material. When Fe is plotted against Mn for this sample, the clusters of points for the modulated and clear regions actually overlap. This seems to indicate that in the Piz Cam kutnahorite, two elements at least (Fe and Mg) locally approach concentration limits, the exceeding of which leads to single-phase instability.

Manganoan calcite. Within some of the kutnahorites there occur grains which have the $R\bar{3}c$ structure. They are essentially manganoan calcite. Like the ferroan calcites, they tend to suffer deterioration under the electron beam (although not so rapidly) and small, platelike precipitates and dislocation loops which are often seen in these calcitic grains (paralleling the situation in ferroan calcite—Barber and Wenk, 1984) tend to develop during irradiation. A ribbon-like coherent second phase sometimes occurs in these grains of manganoan calcite. The fringe contrast exhibited by these ribbons, coupled with occasional occurrences of moiré fringes and superstructure diffraction spots, suggest that the ribbons are dolomite-structured.

Siderite

The two siderites examined came from Erzberg, Styria, Austria (no. 4372) and from Cornwall, England. Of these the most interesting proved to be that from Erzberg. The average composition of this siderite, determined by TEM/EDS analysis, was 87.5 wt. % FeO, 8.0% MgO, 3.8% MnO, 0.7% CaO. Minor grains of calcite, leucite, quartz and hematite occurred within the sample. The siderite mostly exhibits a moderate-to-high density of curved dislocations and loops. Siderite is stable under the electron beam, unlike the calcite which is ferroan and displays the tendency to beam damage that is characteristic of impure calcites. Although at first sight BF images indicate that the siderite is single phase, DF images such as that shown in Fig. 6a reveal the presence of faint fringes defining ribbon-like defects, which suggest that it has some very small, thin laths of second phase.

Siderite grains which are contiguous with calcite are perhaps the most interesting. These display twisting and curving ribbon-like defects, which branch repeatedly nearer to the calcite grains, as shown in Fig. 6b. Although one end of a ribbon

sometimes terminates at a dislocation, this is not necessarily the case. The fringes displayed by the defects in BF and DF images are essentially

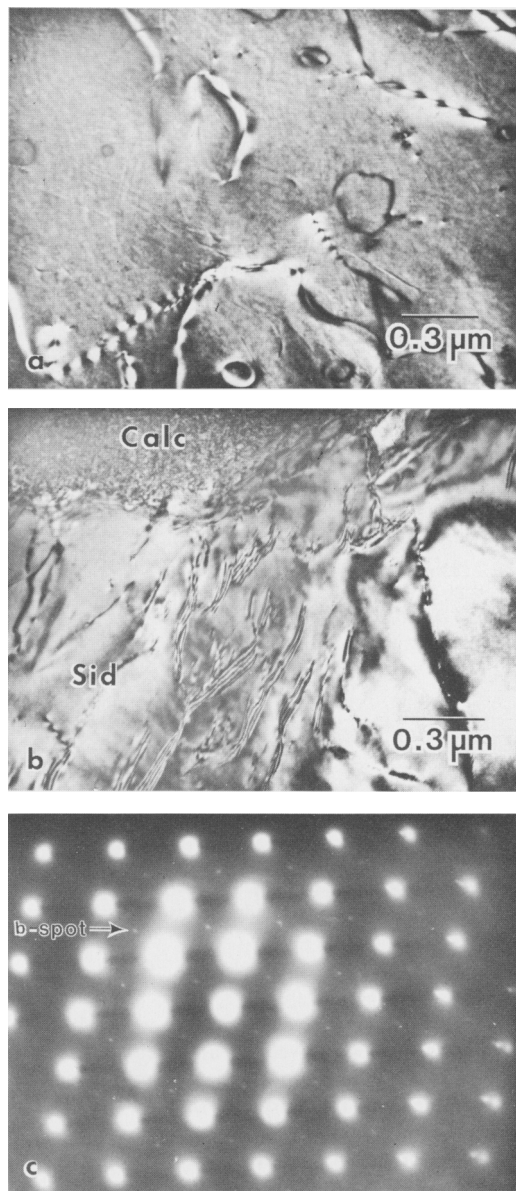


FIG. 6. (a) DF image showing dislocations and faint ribbon-like fringed images in Erzberg siderite. (b) BF image showing branching ribbons in a region of the Erzberg siderite adjacent to a grain of calcite. (c) Diffraction pattern from Erzberg siderite, showing *a*- and *b*-type spots. Note the splitting of high-order spots.

complementary and behave similarly to those shown by calcitic ribbons of second phase in dolomite (King *et al.*, 1984; Barber *et al.*, 1985). When the field aperture is placed over regions which have high ribbon densities, the diffraction pattern thus formed shows *b*-type reflections, as illustrated in Fig. 6c, which are not to be expected from siderite. In addition to the *b*-type spots, 0003 and 0009 along the c^* row, high-order reflections (e.g. 00012) show small splittings. When the specimen is tilted away from a zone-axis orientation about an axis parallel to c^* , the difference in intensity between the $l = \text{odd}$ and $l = \text{even}$ spots is unchanged, showing that the $l = \text{odd}$ spots are indeed superlattice spots and not the result of double diffraction. Comparing diffraction patterns from ribbon-dense areas with those from ribbon-poor areas, it was noted that the *b*-type spots were more intense in the former. The diffraction information clearly indicates that the ribbons consist of a second phase which has an $R\bar{3}$ symmetry.

Using the 'average composition' method of microanalysis it was further found that the ribbon regions were richer in Ca than their Fe-bearing surroundings. This is clearly demonstrated by the plots of Fe versus Ca content shown in Fig. 7. for both clear regions and regions containing the ribbons. The same sets of data also show that the ribbon regions contain less Mg and more Mn than the adjacent clear regions. Taking the diffraction results together with the analytical data we con-

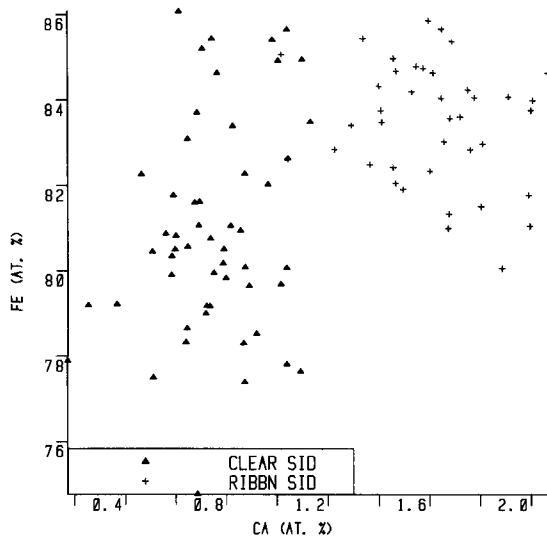


FIG. 7. Graph showing plots of Fe versus Ca obtained from TEM/EDS microanalyses of 'clear' and 'ribbon' regions in the Erzberg siderite.

clude that the ribbons in siderite have the dolomite structure.

The calcite grains within the Erzberg siderite also exhibit a number of interesting effects. They are ferroan ($\text{FeO} \approx 4$ wt. %) and tend to damage rapidly on electron irradiation, which causes the appearance of many dislocation loops. Electron diffraction patterns from this calcite, as typified by Fig. 8a, show diffuse scattering along the $\langle 10\bar{1}4 \rangle$ directions in reciprocal space and, more surprisingly, diffuse *c*-type reflections. Apart from the case of oolitic calcite (Gunderson and Wenk, 1981), *c*-type reflections have previously been found only with $R\bar{3}$ carbonates. Even more unusual is the finding that the *c*-type spots occur in all three possible reciprocal lattice directions for a given zone, whereas Gunderson and Wenk have pointed out that the *c*-type reflections which they observed occurred at the half distance between only one of

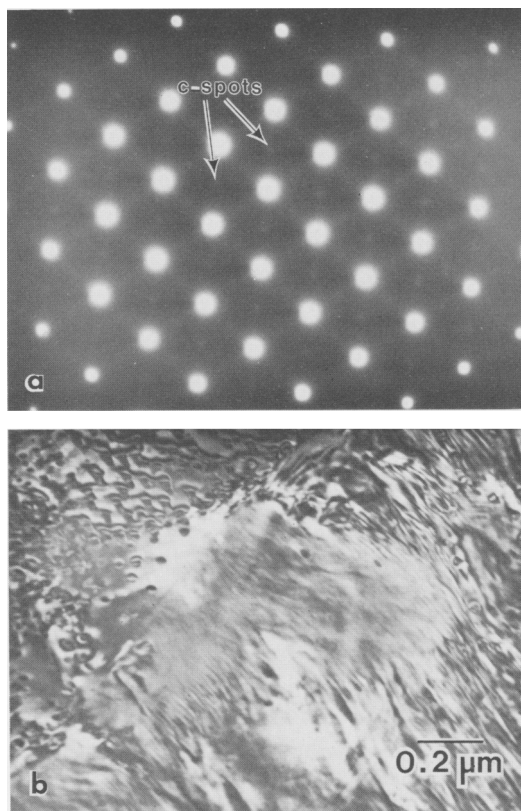


FIG. 8. (a) Diffraction pattern from calcite within Erzberg siderite, showing *c*-type spots and diffuse scattering. (b) Striated region in calcite within Erzberg siderite. Note the (more usual) appearance of plate-like precipitates in the top left corner.

the possible sets of *a*-type spots. (In terms of the models proposed by Reeder and Wenk, 1979*b*, and Van Tendeloo *et al.*, 1985, this appears to imply ordering of cations in rows parallel to only one of the three possible directions lying within the basal plane.) Striated microstructures also occur in some regions of the calcite, as shown in Fig. 8*b*. Microanalysis indicates that such regions contain abnormally high amounts of Mn and Fe.

The observation of composition-related modulated microstructures in the calcite seems to suggest that its composition sometimes comes close to the limits of solid solubility. This idea seems to be borne out by the finding of fringed, lath-like defects in some of the calcite grains. These laths, which are less twisted or curved than the ribbons in the siderite, are illustrated in Fig. 9*a* and *b*. Their fringe and diffraction properties are otherwise similar to the fringed defects already described as occurring in rhombohedral carbonates. The laths appear bright in DF images formed using *either* the *b*- or *c*-type spots which occur in diffraction patterns from these areas, as typified by Fig. 9*c*. When *c*-type spots are used for imaging, other fine lamellae are also visible in the calcite background. Diffraction patterns from lath-free areas of the ferroan calcite have *c*-type spots, but no *b*-type spots. These *c*-type spots are often streaked and their elongation is in the same direction as the splitting of *a*-type spots in diffraction patterns from lath-dense regions. We also note that the *c*-type spots occurring between two *b*-type spots are stronger than the *c*-type spots between two *a*-type spots.

When average composition data for Ca and Fe concentrations are plotted for both the clear and the ribbon-containing regions of the calcite, a strong trend is seen, as illustrated in Fig. 10*a*. The ribbons are clearly associated with a high concentration of Fe. If we had also plotted regions with lower ribbon densities, the data points would have fallen on the same line. The Mn concentration in the clear calcite is variable, as shown in Fig. 10*b*, and some of the calcite is strongly manganoan. The Mn concentration in the ribbon regions has a smaller spread. The Mg concentration shows the reverse behaviour, i.e. it is higher in the ribbon regions than in the clear calcite. Thus in both the siderite and the calcite, the Mg ions show siderophilic behaviour.

It is apparent from the above observations that the second-phase laths in the calcite are coherent with it, but differ in both lattice parameters and composition. The appearance of the *b*-type spots, in addition to the diffuse *c*-type spots shown by the calcite, shows that the second-phase laths have $R\bar{3}$ symmetry. Therefore the laths cannot be siderite. Taken in conjunction with TEM/EDS data, we

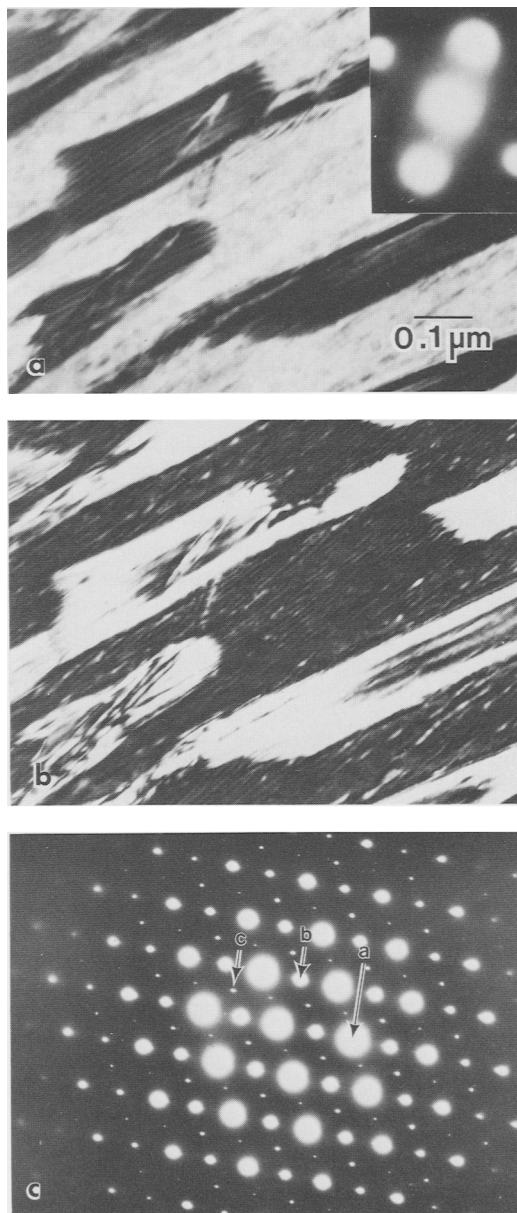


FIG. 9 (*a* and *b*). BF and DF images of laths of second phase in the calcite within the Erzberg siderite. $10\bar{1}4$ reflection. (*c*) Zone axis diffraction pattern corresponding to (*a*) and (*b*), showing *a*-, *b*- and *c*-type spots.

thus conclude that they are dolomitic material, probably ankerite since the phase $\text{FeCa}(\text{CO}_3)_2$ has never been identified in minerals and cannot be synthesized (Rosenberg and Foit, 1979).

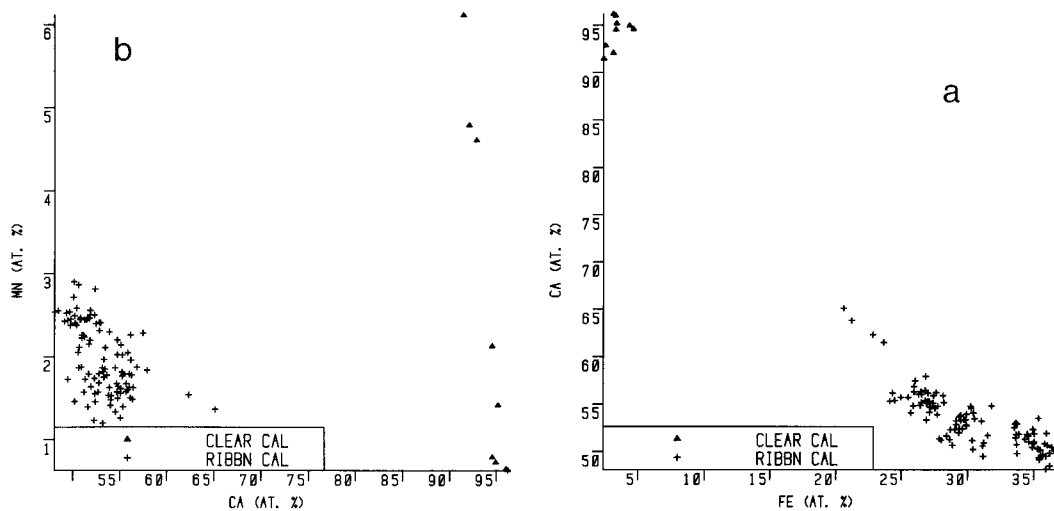


FIG. 10 (*a* and *b*). Graphs showing (*a*) Ca versus Fe, and (*b*) Mn versus Ca obtained from TEM/EDS microanalyses of ribbon-containing and clear regions of calcite in the Erzberg siderite.

Smithsonite

Samples of smithsonite from three different localities have been examined. These came from Tsumeb, south-west Africa (BM 1968, 688), Broken Hill, Kopje No. 5, Zambia (BM 1929, 1754) and an unknown location in Mexico. The principal metallic impurities in these samples were Fe, Ca, Mg and Cu. It was therefore necessary, exceptionally, to mount specimens on nickel grids to facilitate microanalysis. An additional problem with this mineral is its tendency to damage rapidly during electron irradiation, especially when it contains significant amounts of Cu or Ca.

All three samples contained ubiquitous, modulated microstructures and, in many regions, strong growth banding. Figs. 11*a* and *b* from Tsumeb and Broken Hill, respectively, give some idea of the types of modulated microstructures encountered. These images have strong similarities to those obtained from calcian dolomites (Reeder and Wenk, 1979*a, b*) and some calcites (Gunderson and Wenk, 1981; Wenk *et al.*, 1983). However, no *c*-type spots have been observed in diffraction patterns from any of the samples, even after long exposure times. The *a*-type spots, to be expected from an $R\bar{3}c$ carbonate, are diffuse and, in patterns from strongly modulated regions, are elongated in a direction perpendicular to the trace of the modulations.

The growth bands, which are easily visible in the optical microscope, are also very striking when imaged in the electron microscope, as illustrate by Fig. 12*a*, which shows the Mexican sample. The bands are strongest where Cu occurs as a major

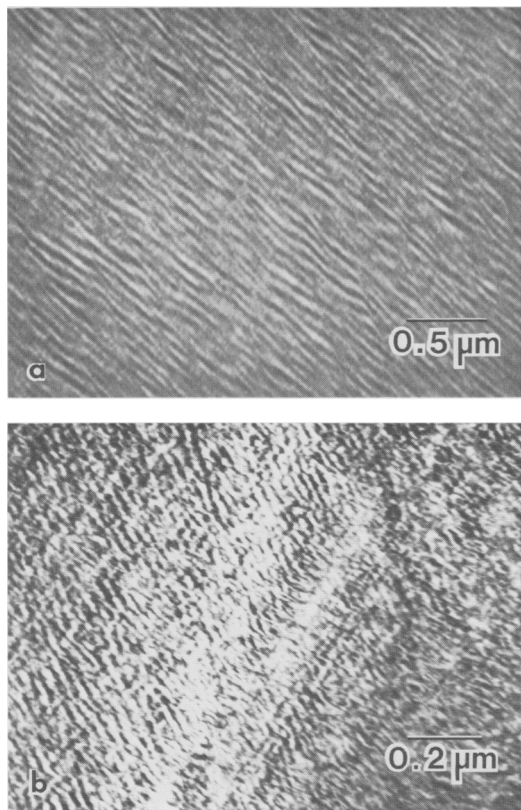


FIG. 11 (*a* and *b*). Illustrating striated and modulated microstructures in smithsonites from (*a*) Tsumeb, (*b*) Broken Hill, respectively.

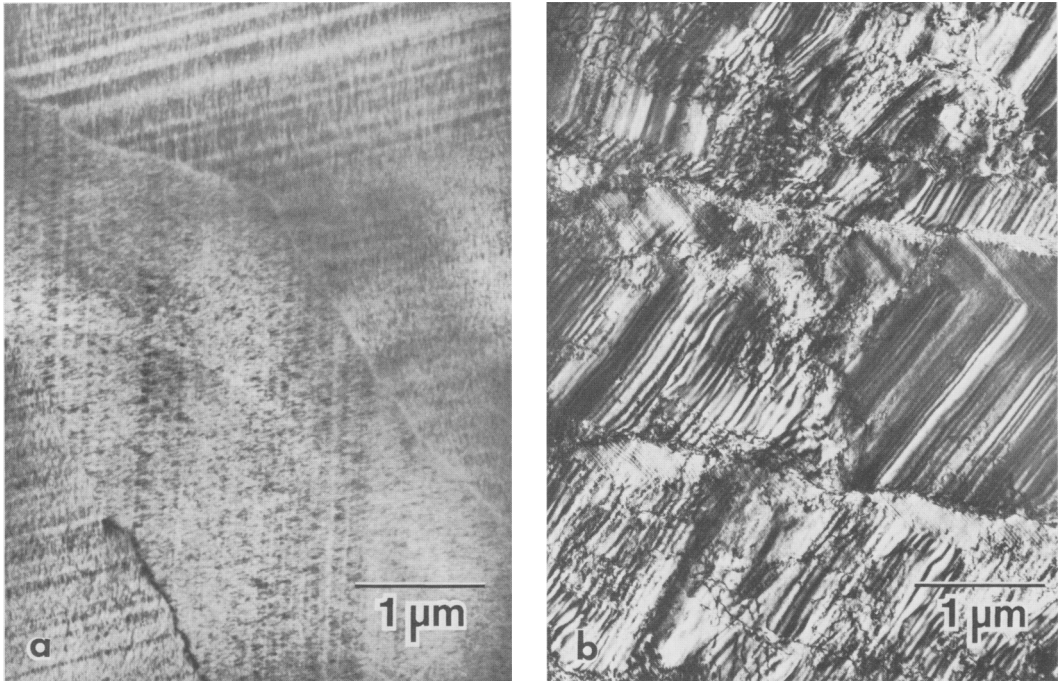


FIG. 12. (a) Growth bands and modulations in Mexican smithsonite. (b) Strong growth bands, sector boundaries with walls of dislocations and modulations in copper-rich zone of Mexican smithsonite.

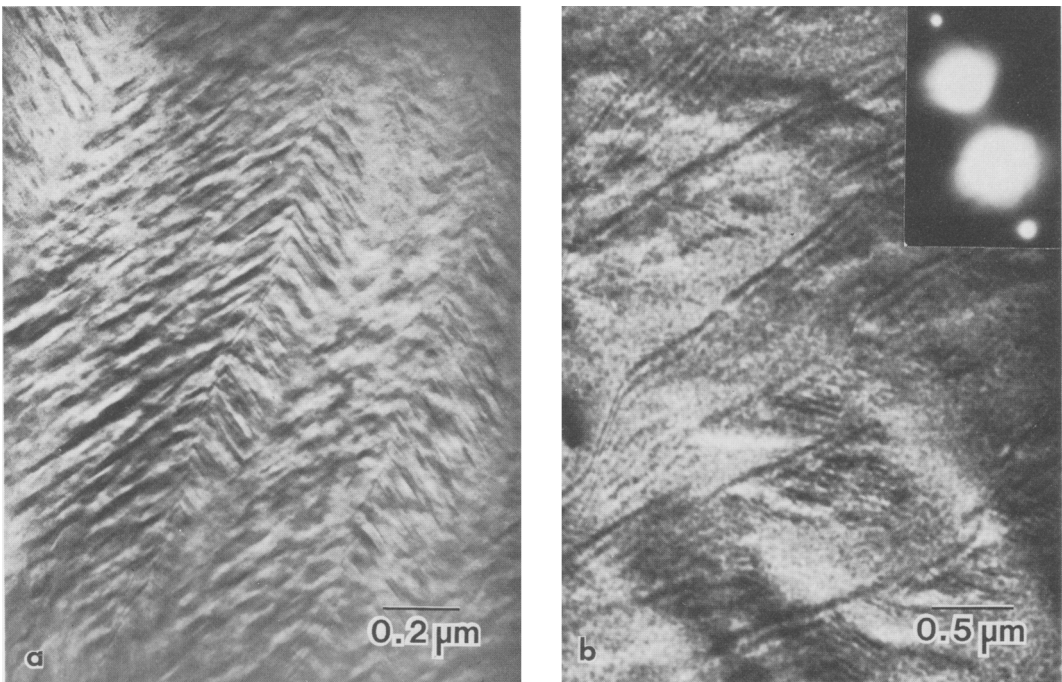


FIG. 13. (a) Dendrite-like striations in Broken Hill smithsonite. (b) DF image of fringed ribbons with side branches in Tsumeb smithsonite. 0006 reflection.

impurity, in the zones of contact with adjoining minerals, which tend to be even richer in Cu than the smithsonite. The microstructure of the growth bands consists mainly of (i) growth sector boundaries, which represent small lattice misorientations ($\approx 1^\circ$) and therefore usually take the form of walls of dislocations; (ii) fringed, lathlike defects (see Fig. 12*b*); (iii) regular modulations in contrast, which apparently relate to ancient growth fronts, to judge by their shapes in relation to crystallite boundaries, as illustrated by Fig. 12*b*.

Other features are found which have similarities, at least, to the dendrite-like forms of second phase sometimes found in dolomite from carbonatite. Compare, for example, the feature with the central spine shown in Fig. 13*a* in a specimen of Broken Hill smithsonite with the dendrite shown in Fig. 5*B* of Barber and Wenk, 1984. Fringed defects seen in Fig. 13*b*, from the Tsumeb sample, have short fringed side arms, very similar to many of the second-phase ribbons found in saddle dolomite (see for example, Fig. 1*D* in Barber *et al.*, 1985). No *b*-type spots have been found in diffraction patterns from these regions displaying ribbon-like features.

Some grains in the Tsumeb smithsonite have only Fe as a divalent impurity. In these grains there is a high density of fringed structures and the density is directly dependent on the local Fe content. TEM/EDS microanalysis, using the average composition method, has again enabled us to relate changes in microstructure with changes in the concentrations of divalent impurity ions. As an illustration, Fig. 14 shows a plot of Ca concentration versus Zn from analyses of the sample from Zambia. The graph shows that modulated microstructures appear as the concentration of Ca increases and that yet higher local concentrations of Ca are associated with regions exhibiting both modulations and growth bands. (No cations other than Ca and Zn were detected for the data points on the right side.) Similar trends have been found for other divalent cationic impurities in the other samples of smithsonite.

Rapid beam damage of the smithsonite, which produces a spotty background contrast, makes it difficult to see the fine detail of many features. We nevertheless conclude that lattice-coherent, second-phase ribbons occur in smithsonite and that these are especially associated with high concentrations of Ca, Cu and Fe impurities. Since no diffraction spots indicative of $R\bar{3}$ symmetry appear, we conclude that the second phases have $R\bar{3}c$ symmetry.

Synthesized carbonates

Some work has been carried out on two systems, $MgCO_3$ - $CdCO_3$ and $CaCO_3$ - $MnCO_3$ both of

which should, in principle, enable an $R\bar{3}$ ordered dolomite to be synthesized at temperatures below 1000°C . Our main efforts are now being centred on the second system, because it also disorders at very low temperatures (see Introduction), and offers the best prospects for studying how composition, temperature of annealing, etc. affect the degree of order. Materials synthesized to date have been heterogeneous, both from the viewpoint of composition and microstructure. The problem seems to be largely one of mixing and homogeneity prior to heat treatment. The specimens that we have examined by TEM have been taken from regions which have been judged from optical studies of thin sections to be the most reacted.

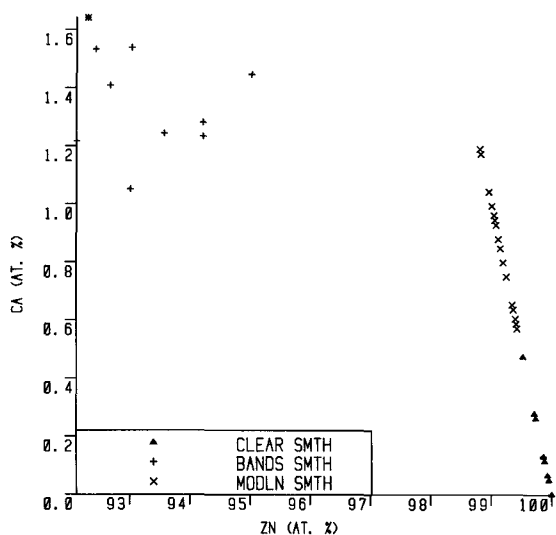


FIG. 14. Graph showing Ca versus Zn concentrations obtained from TEM/EDS microanalyses of 'banded-', 'modulated-' and 'clear-' regions in the Zambian smithsonite.

Fig. 15*a* shows part of a grain of Cd-dolomite that contained dislocations, but showed no evidence of compositional modulations. The diffraction pattern (inset) shows both *a*- and *b*-type reflections, which, although there is some splitting of high order *a*-type spots, indicates that most of the volume has the dolomite structure. But other nearby grains within the same sample contained features which appeared to be irregular compositional variations.

The results of our experiments with the $CaCO_3$ - $MnCO_3$ system seem to confirm earlier findings that Mn ions can be accommodated with ease in the

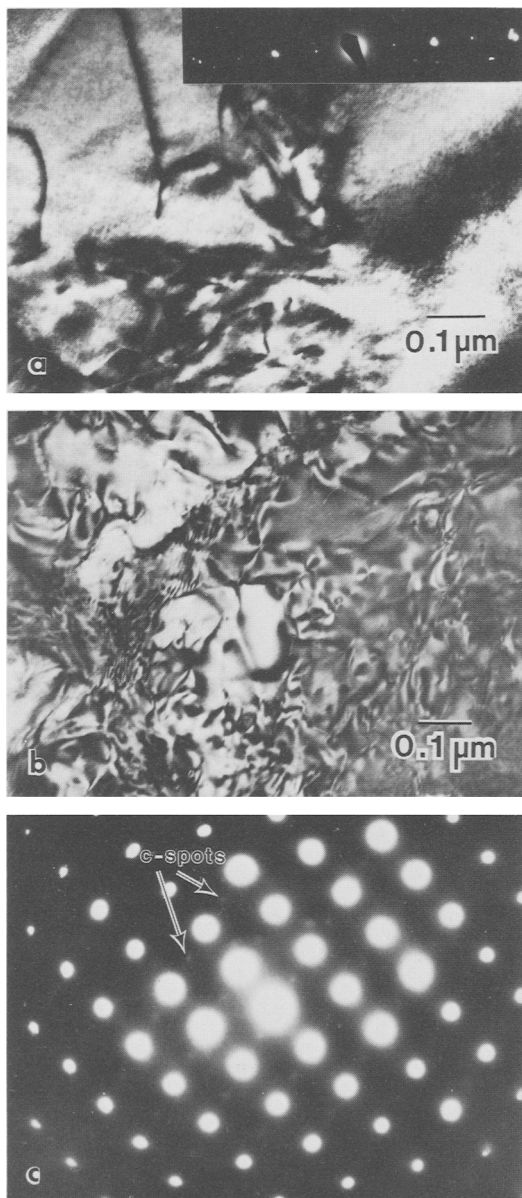


FIG. 15. (a) Microstructure in unstrained grain of synthetic Cd-dolomite. Note splitting of high-order diffraction spots of c^* systematic row (inset), indicating two-phase nature. (b) Microstructure in grain of synthetic manganese calcite. Note effect of internal strain from defects on diffraction contrast. (c) Diffraction pattern from synthetic manganese calcite, showing c -type spots.

calcite structure and we have not yet synthesized any material with a sufficiently high Mn content to induce the appearance of the dolomite variant.

TEM/EDS analysis shows that heat treatment at 550 °C for 24 hr (without recrystallization) causes ~ 16 at. % Mn to be introduced into the calcitic grains. Higher sintering temperatures produce larger Mn contents, with ~ 35 at. %, corresponding to a temperature of 650 °C and the same time. The manganese calcites are highly strained, as shown by Fig. 15b, and this makes it difficult to discover the nature of the faults that are present. As already implied, b -type reflections have not been observed in any synthetic sample, but diffraction patterns from such regions, as shown in Fig. 15b, invariably exhibit c -type reflections, as shown in Fig. 15c. This finding, if interpreted in terms of the model of Van Tendeloo *et al.* (1985) implies that the Ca and Mn ions order within individual basal cation layers.

Discussion and conclusions

The results show that particular impurity-related microstructures, previously reported to occur in a few types of rhombohedral carbonate (Reeder and Wenk, 1979a, b; Wenk *et al.*, 1983; Barber and Wenk, 1984; Barber *et al.*, 1985), occur in a wider variety of carbonates, having differing origins and chemistries. The principal types of microstructure can be grouped into four main categories, namely: (i) thin sheets of second phase (see in TEM as ribbons or laths); (ii) wave-like or modulated microstructures, whose nature remains uncertain, but which appear to represent regular, fine-scale compositional variations; (iii) small lenticular precipitates, principally associated with the occurrence of Ca or Fe as impurities in $R\bar{3}c$ carbonates; (iv) growth bands, which are often accompanied by (ii), and are found mainly in samples with low-temperature origins. Type (ii) microstructures, first reported in calcian sedimentary dolomites (Reeder and Wenk, 1979a, b), have now been shown by our results to occur in close proximity to type (i) microstructures. The interpretation of the latter is now fairly clear, since our findings in ankerites, siderites and kutnahorites all support the views (Barber and Wenk, 1984; Barber *et al.*, 1985) that the ribbon-like and lath-like defects are second-phase carbonate, coherent with the host carbonate. A new finding is that the $R\bar{3}$ second phase in an $R\bar{3}c$ host may also take this form, as indicated by the ribbons in siderite. It has, however, been known for some time (Goldsmith, 1960) that the dolomite exsolved from calcite can be epitactic, while Puhani (1984) has illustrated one coherent, dendritic form. Our observations on the Neudorf ankerite show that the second phase can be strongly interconnected, to form a cellular structure of sheets. The types (iii) and (iv) microstructures are also fairly straightforward to interpret, the former being described by

Barber and Wenk (1984) and the latter by Reeder (1983*b*). Unfortunately, a more precise interpretation of the type (ii) modulated microstructures still eludes us, despite the proximity of types (i) and (ii) in some samples and indirect compositional evidence contained in this paper that type (i) microstructures may result from the evolution of type (ii).

It would be premature, in general, to attempt to draw any firm conclusions from the existence of particular types of microstructure in carbonates with particular impurities. More extensive investigations of particular systems are needed, aided by the use of synthetic carbonates when an adequate range of compositions cannot be covered with natural samples. Possible reasons for the destabilization of the dolomite and calcite structures have been advanced by several groups.

Rosenberg and Foit (1979) and Effenberger *et al.* (1981) have suggested that excessive trigonal distortion of octahedral sites is a critical factor for the dolomite structure and hence give a list of cations that will, when placed in the Mg sites, lead to increasing instability. This predicts that increasing the Fe/Mn ratio in kutnahorite tends to destabilize, which seems to be supported by our results. Rosenberg and Foit also comment on the absence of an ordered compound $\text{CaFe}(\text{CO}_3)_2$. Goldsmith (1960) provided data on the occurrence of Fe in calcite and showed that although ~ 30 mole % Fe could exist in solid solution at 700°C , only 5 mole % could be retained in solution at 300°C . We note that ferroan calcites are extremely unstable under electron irradiation and have obtained further evidence (see Barber and Wenk, 1984) that small, apparently pre-existing plate-like precipitates in such calcites grow during irradiation. This may cast doubt on published solubility limits, which have been determined by low resolution methods. We have no evidence for the existence of $\text{CaFe}(\text{CO}_3)_2$, even as thin laths, in Ca-bearing siderite, but we note that the laths are dolomitic in nature (since they cause *b*-type reflections) and they do contain a high concentration of Fe, as deduced from the trends shown by our graphs of compositional data.

We also note the occurrence of *c*-type reflections and streaks of diffuse scattering from the calcite occurring in the siderite samples. This calcite (which contained not only Fe but also Mg and Mn) could be interpreted (in terms of the model of Van Tendeloo *et al.*, 1985) as indicative of Ca, Fe ordering in the basal plane. The positions of these *c*-type order spots in various zones suggests that both the *a* and *c* lattice-parameters are doubled. The results of Wenk and Fusheng (1985) show that heat treatment destroys *c*- and *d*-type spots and any diffuse streaking and, by inference, associate these

diffraction effects with local order. Recently Kucha and Wiczorek (1984) have reported results on ankerites from the Erzberg and Radmer-Buchegg mines, Austria, which they have interpreted as evidence for periodic, antiphase structures. Their electron-diffraction patterns show spot-spitting suggestive of two-phase effects similar to those which we find in some ankerites. They deduce that calcite is one of the 'antiphase units' but they also surprisingly suggest that another is $\text{CaFe}(\text{CO}_3)_2$, with an upper size limit for these domains of 20–40 nm.

The occurrence of *c*-type reflections in a number of our samples with very different compositions was not anticipated and needs further study. The streaking observed in *c*-type spots is usually parallel to the direction in which *a*-type spots are split and could be ascribed to variations in lattice parameters resulting from compositional heterogeneities. But we also note that the *c*-type spots which lie between *b*-type spots are more intense than the *c*-type spots which lie between *a*-type spots (see Fig. 9*c*). And there are other unexplained results. In particular, we find it surprising that the synthetic Ca–Mn, $R\bar{3}c$ carbonates that we have prepared exhibit *c*-type reflections, but that Ca–Mn calcitic grains in the natural kutnahorites do not show them. Another notable difference is that the natural minerals are prone to damage during electron irradiation whereas the synthetic materials of similar composition are not.

The calcite-dolomite solvus and the effect of minor elements upon it (particularly Fe) is important in relation to geothermometry of limestones (Barron, 1974; Bickle and Powell, 1977) and carbonatites (Gittins, 1979). In this respect alone, a better knowledge of the nature of two-phase effects in carbonates and the effects of rock composition upon them is important. It is clear from our results that the scale of much of the second phase is only accessible to electron-optical methods and, most easily, to TEM methods. Only where the carbonate second phase is very dense and pervasive is its presence detectable by means of the lustre and turbidity of the sample. These points seem to cast some doubt on the reliability of calcite-dolomite geothermometry at this stage of knowledge.

Equally encouraging, however, is the prospect that analytical TEM methods are capable of giving direct information about the limits of solid solubility, the occurrence and nature of intermediate phases, order-disorder, etc. Considerable progress has been made in understanding the microstructures in rhombohedral carbonates in the last few years using TEM and HREM (Wenk *et al.*, 1983). Analytical TEM demonstrably also has an important role to play.

Acknowledgements

We thank Drs A. M. Clark (British Museum, Natural History), L. Zak (Charles University, Prague) and H. R. Wenk (University of California, Berkeley) for kindly supplying samples. We also thank T. G. Goodwin for technical assistance, and C. Alexander for the computer program used to produce Figs. 5, 7, 10 and 14. Both R. J. Reeder and an anonymous referee made comments which led to improvements in the manuscript. One of us (M.R.K.) thanks the University of Peshawar, Pakistan, for study leave and the Government of Pakistan for a scholarship. The work was supported by the Natural Environment Research Council.

References

- Barber, D. J. and Wenk, H. R. (1984) *Contrib. Mineral. Petrol.* **88**, 233–45.
- Reeder, R. J. and Smith, D. J. (1985) *Ibid.* **91**, 82–92.
- Barron, B. J. (1974) *Ibid.* **47**, 77–80.
- Bickle, M. J. and Powell, R. (1977) *Ibid.* **59**, 281–92.
- Cliff, G. and Lorimer, G. W. (1975) *J. Microsc.* **103**, 203–7.
- Effenberger, H., Mereiter, K. and Zemann, J. (1981) *Z. Kristallogr.* **156**, 233–43.
- Goldsmith, J. R. (1960) *J. Geol.* **68**, 103–9.
- (1983) In *Rev. in Mineralogy* **11** (R. J. Reeder, ed.) Mineral. Soc. America.
- Gittins, J. (1979) *Contrib. Mineral. Petrol.* **69**, 1–4.
- Gunderson, S. H. and Wenk, H. R. (1981) *Am. Mineral.* **66**, 789–800.
- King, A. H., Chen, F. R., Reeder, R. J. and Barber, D. J. (1984) *Proc. 42nd Mtng EMSA* (G. W. Bailey, ed.) San Francisco Press, Inc.
- Kucha, H. and Wiczorek, A. (1984) *Tschermaks Mineral. Petr. Mitt.* **32**, 247–58.
- Lloyd, R. V., Lumsden, D. N. and Gregg, J. M. (1985) *Geochim. Cosmochim. Acta* **49**, 2565–8.
- Puhan, D. (1984) *Contrib. Mineral. Petrol.* **87**, 98–9.
- Radke, B. M. and Mathis, R. L. (1980) *J. Sed. Petrol.* **50**, 1149–68.
- Reeder, R. J. (1981) *Contrib. Mineral. Petrol.* **76**, 148–57.
- (1983a) In *Rev. in Mineralogy* **11** (R. J. Reeder, ed.) Mineral Soc. America.
- (1983b) *Estudios Geologicos* **38**, 179–83.
- and Wenk, H. R. (1979a) *Geophys. Res. Lett.* **6**, 77–80.
- (1979b) In *Modulated Structures—1979* (J. M. Cowley *et al.*, eds.) American Inst. Physics.
- Rosenberg, P. E. and Foit, F. F. (1979) *Geochim. Cosmochim. Acta* **43**, 951–5.
- Van Tendeloo, G., Wenk, H. R. and Gronsky, R. (1985) *Phys. Chem. Minerals* **12**, 333–41.
- Von Eckermann, H. (1948) *Sverig. Geol. Undersok.*, Ser. Ca., No. 36.
- Wenk, H. R. and Fusheng, Z. (1985) *Geology* **13**, 457–60.
- and Maurizio, R. (1978) *Schweiz. Mineral. Petrogr. Mitt.* **58**, 97–100.
- Barber, D. J. and Reeder, R. J. (1983) In *Rev. in Mineralogy* **11** (R. J. Reeder, ed.) Mineral. Soc. America.
- Wood, J. E., Williams, D. B. and Goldstein, J. I. (1984) *J. Microsc.* **133**, 255–74.
- Zak, L. and Povondra, P. (1981) *Tschermaks Mineral. Petr. Mitt.* **28**, 55–63.

[Revised manuscript received 4 July 1986]